SUPPLEMENTAL MATERIAL

1. Microtubule mechanics

The relaxation time of a bent microtubule in a viscous fluid can be estimated from the equation of motion for small displacements, u, from the straight configuration (Love, 1944; Landau and Lifshitz, 1986);

$$m\ddot{u} + \xi\dot{u} + Bu'''' = 0, \tag{S1}$$

where m is the mass per unit length of the filament, ξ is the frictional resistance per unit length, and $B \simeq 25\ \mathrm{pN}\ \mu\mathrm{m}^2$ (Howard, 2001) is the flexural rigidity. The solutions are a linear combination of trigonometric and hyperbolic functions with a wavevector k. For a free-ended segment in the lowest energy mode $kl = 1.875$; thus, for a typical segment length $(l \simeq 3\ \mu\mathrm{m})$ $k \simeq 0.6\ \mu\mathrm{m}^{-1}$. Neglecting inertia, in the overdamped limit the relaxation time is given by

$$\tau = \frac{\xi}{Bk^4}. \tag{S2}$$

The frictional resistance is given by $\xi = 4\pi\mu/\ln 2A$, where μ is the effective viscosity of the background fluid and the aspect ratio of the segment $A \simeq 120$. Estimates of the viscosity of cellular fluids range from 10^{-3} Pa s (water) to 10^{-1} Pa s (Fushimi and Verkman, 1991; Bicknese *et al.*, 1993) and the corresponding relaxation times for $3\ \mu\mathrm{m}$ segments are in the range 10^{-3} – 10^{-1} s. Observations of microtubule straightening in dynein inhibited cells indicate that the effective viscosity controlling the relaxation of microtubules is much larger. We take a value $\mu = 10$ Pa s, which gives a relaxation time of approximately 7 s for a $3\ \mu\mathrm{m}$ segment, similar to the experimental data in Figure 1A.

2. Model for dynein forces

In this model, the force exerted by a dynein molecule is assumed to depend on the displacement of the motor from the point of attachment to the microtubule (in a space-fixed frame), and has contributions from the motion of the microtubule as well as the motor. Individual dynein molecules walk toward a microtubule minus end at a speed v_m that depends on the opposing force, $\mathbf{f}$. For simplicity, the force-speed relation for dynein motors is taken as linear (Toba *et al.*, 2006),

$$\frac{v_m}{v_0} = 1 - \frac{\mathbf{t}.\mathbf{f}}{f_{max}}, \tag{S3}$$

where v_0 is the speed of an unstressed motor, f_{max} is the motor stall force, and $\mathbf{t}$ is a unit vector directed toward the plus end of the microtubule. The force on the cytomatrix linkage increases as dynein translates and begins to exert tension, while motion of the microtubule itself can also contribute to a change in force. Assuming that the dynein-linkages can be approximated as linear springs with stiffness κ,

$$\frac{d\mathbf{f}}{dt} = -\kappa(\mathbf{v} - v_m\mathbf{t}) \tag{S4}$$

where $\mathbf{v}$ is the local velocity of the microtubule relative to the cytoskeleton. The time-dependent force from a single motor follows from Equations (S3) and (S4) with the initial condition $\mathbf{f}(0) = 0$;

$$\mathbf{f}(t) = f_{max}\left(1 - \frac{\mathbf{v}\cdot\mathbf{t}}{v_0}\right)\left(1 - \mathrm{e}^{-t/\tau}\right)\mathbf{t} - \kappa\mathbf{v}\cdot(\mathbf{1} - \mathbf{tt})\,t, \tag{S5}$$

where the timescale for the motor to stall $\tau = f_{max}/\kappa v_0$. Typical values for the parameters are: $\kappa = 1000\ \mathrm{pN}\mu\mathrm{m}^{-1}$, $v_0 = 0.8\ \mu\mathrm{m\ s}^{-1}$, and $f_{\max} = 8\ \mathrm{pN}$ (Howard, 2001; Toba *et al.*, 2006), leading to a timescale $\tau = 0.01s$.

Dynein linkages between the cytomatrix and the microtubule are assumed to dissociate with a first-order rate constant k_{off}, so that the probability of a linkage remaining at time t is $P(t) = e^{-k_{off}\,t}$. Thus the average force exerted by a single linkage over a time interval T is $\langle \mathbf{f}_l \rangle = T^{-1} \int_0^T \mathbf{f}(t) P(t) dt$. The mean linkage lifetime is ${k_{off}}^{-1}$and thus there are $k_{off} T$ linkages broken and reformed in the time interval T. The average force exerted by a dynein linkage that is associating and dissociating from the microtubule is therefore

$$\langle \mathbf{f} \rangle = k_{off} \int_0^\infty \mathbf{f}(t) P(t) dt = f_0 \left(1 - \frac{\mathbf{v} \cdot \mathbf{t}}{v_0}\right) \mathbf{t} - \frac{\kappa}{k_{off}} \mathbf{v} \cdot (\mathbf{1} - \mathbf{tt}), \qquad \text{(S6)}$$

where $f_0 = f_{max}/\left(1 + k_{off}\tau\right)$ is the average force per linkage on a stationary actomyosin cortical network. The best estimate of the dynein off rate is $k_{off} \sim 1\text{s}$, so that the mean motor force is essentially the same as the maximum force, $f_0 \simeq f_{max}$. The force per unit length of the microtubule, $\mathbf{K}$, can then be obtained by multiplying Equation (S6) by the density of dynein linkages per unit length, ρ,

$$\mathbf{K} = \rho \langle \mathbf{f} \rangle = \rho f_0 \left(1 - \frac{\mathbf{v} \cdot \mathbf{t}}{v_0}\right) \mathbf{t} - \rho\gamma \mathbf{v} \cdot (\mathbf{1} - \mathbf{tt}) \qquad \text{(S7)}$$

where $\gamma = \kappa / k_{off}$ is the friction coefficient for lateral motion per dynein linkage.

3. Simulation methods.

The numerical simulations are based on an algorithm for integrating the equations of motion of an elastic filament (Ladd and Misra, 2009). In addition, we include length changes in the microtubule to incorporate polymerization and depolymerization of the microtubules. The length of the microtubule is taken to be a continuous variable, described by a stochastic differential equation that includes switches to catastrophe (depolymerization) and recovery (polymerization). The parameters are taken from experimental measurements (Gliksman *et al.*, 1993; Shelden and Wadsworth, 1993): $v_{pol} = 0.1\ \mu\text{m s}^{-1}$, $v_{depol} = 0.3\ \mu\text{m s}^{-1}$, $k_{cat} = 0.05 s^{-1}$, and $k_{rec} = 0.2 s^{-1}$. Segments are added or removed from each microtubule during the simulation, according to the calculated changes in length. The model for dynein motors, Equation (S7), is included in the force balance that describes the evolution of each microtubule, Equation (2), which leads to an expression for the microtubule velocity in terms of the coordinates. The conformation of each microtubule is then updated with a time step of the order of 1 μs.

The dynamics of the centrosome were simulated by distributing microtubules around the MTOC with a uniform distribution of angles; the microtubules are coupled to the MTOC by stiff springs. In the experiments on animal cells many of the microtubules are observed to get pinned when they reach the cell boundary; typically these microtubules buckle as shown in Supplemental Figure S6. However it is sometimes observed that the microtubules slide along the cell boundary as shown in Figure S6A and occasionally microtubules apparently stop growing (Supplemental Figure S6B). We include the possibility of microtubule pinning by an angle dependent rate $k \cos\theta$, where θ is the angle between the tangent at the tip of the microtubule and the normal to the cell surface. We take the rate constant $k = 0.2\ \text{s}^{-1}$ and the unpinning rate as k. With this choice of kinetics about 2/3 of the microtubules are pinned at any one time, similar to the experimental observations. The remaining microtubules continue to polymerize as their tips slide along the cell surface. We also reduce the growth rate of pinned microtubules by 50% in comparison with the free microtubules to account for stalling in the polymerization kinetics. However, in simulations of *in vitro* microtubule growth, we allowed the microtubules to slide freely along the surface, mimicking the effect of the smooth glass walls.

4. Simulations of microtubule buckling

The simulation illustrated in Figure 2B models a minus-ended microtubule after severing, corresponding to the experiment shown in Figure 1A. The microtubule is pinned at the plus end, but a similar result would follow from the frictional resistance of an additional segment out of the field of view. The simulation shows a small initial buckle under the action of a continuous distribution of dynein motors. We observe a growth in the amplitude of the buckle with time, and a gradual pushing of the buckle towards the plus end. The simulation reproduces the key features of the experiment shown in Figure 1A and on a similar time scale. Variations in the assumed dynein off rate (k_{off}) would be reflected by corresponding changes in the predicted timescale.

5. Simulations of centrosome centering

Simulations of centrosome centering are illustrated in Figure 3C and 3D and in the Supplemental Movies S3 and S4. We compare the dynamics of a radial array of polymerizing microtubules with and without the forces and friction from the dynein motors. The parameters (motor density, motor friction, and friction from the background fluid) are the same as in the single microtubule simulations. Simulations with motors show that microtubules are heavily buckled near the cell periphery whereas in the absence of motors the wavelengths of the buckled microtubules are much longer. The effect of the motors on centrosome centering is striking as can be seen most easily by comparing Supplemental Movies S3 and S4. With dynein motors pulling the microtubules, the centrosome centers with a time constant of about 10 min but simulations without motors suggest that polymerization forces are unable to center the centrosome under *in vivo* conditions. The centrosome remains essentially in place for the duration of the simulation (100 min).

Supplemental Figure S5 compares simulations of centrosome centering with experimental measurements of the fluctuations in centrosome position. The microtubule network develops by polymerization from a radial array of stubs (see Figure 3C) during the first 5 min of the simulation. After the microtubule network has filled the cell, an initially off-center centrosome moves towards the center with a relaxation time of approximately 12 min (time to decay to $1/e$ of its initial displacement). The relaxation time in animal cells, measured from the autocorrelation function of fluctuations in centrosome position was about 8 min, with a standard deviation of 4 min (determined from 14 trajectories of 1-2 hours each).

We have also simulated *in vitro* centering of an MTOC (microtubule organizing center) to compare with data in Ref. (Holy *et al.*, 1997). In that work it was shown that polymerizing forces could center the MTOC by pushing from the cell boundary. The key changes in the simulation parameters were the cell size (12 μm) and the viscosity of the background fluid (10^{-3} Pa s). In addition we eliminated microtubule pinning at the cell boundaries to model the slippage along the glass wall. The polymerization kinetics were tuned to produce microtubules with average lengths of approximately 20 and 40 μm, again to correspond to the conditions of the experiments. The simulations reproduce the key features of the experiments (Holy *et al.*, 1997); with the shorter (20 μm) microtubules the MTOC centers rapidly (Supplemental Movie S5) but with the longer (40 μm) microtubules it drifts to an off center location (Supplemental Movie S6). It can be seen that the longer microtubules buckle significantly and therefore exert much less force than the shorter ones, which remain more or less straight. Under *in vivo* conditions, with a larger cell (40 μm) and a larger viscosity of the background fluid (> 1 Pa s), polymerization forces are much too small to center the centrosome.

It is interesting to compare the buckling of the microtubules in Supplemental Movie S6 with the *in vivo* simulation without motors (Supplemental Movie S4). Under *in vivo* conditions the microtubules buckle into higher order modes because the friction is so large that they do not

relax to the minimum energy state before the next segment polymerizes, whereas under *in vitro* conditions, with a much smaller viscosity, the microtubules buckle into the lowest order mode.

6. Centrosome relaxation time

The centrosome relaxation time can be estimated based on a model of linear rigid microtubules. Assuming each microtubule is pinned at the cell periphery and the centrosome is moving with a velocity $\mathbf{v}_c$, the lateral velocity of the microtubule segment at a distance l from the periphery is $(\mathbf{1} - \mathbf{tt}) \cdot \mathbf{v}_c l/L$, where L is the (time-dependent) contour length of the microtubule; the tangential velocity is assumed to be constant since the microtubule is rigid. The force exerted on the centrosome from a single microtubule is then found by integrating over the contour length,

$$\mathbf{F}_i = \rho f_0 L_i \mathbf{t}_i \left(1 - \frac{\mathbf{v}_c \cdot \mathbf{t}_i}{v_0}\right) - \frac{\rho\gamma L_i}{2} \mathbf{v}_c \cdot (\mathbf{1} - \mathbf{t}_i\mathbf{t}_i) \qquad \text{(S8)}$$

Balancing the forces on the centrosome gives the velocity**,**

$$\mathbf{v}_c = \left\{\sum_i f_0 L_i \mathbf{t}_i\right\} \Big/ \left\{\sum_i \left(\frac{f_0 L_i}{v_0}\mathbf{t}_i\mathbf{t}_i + \frac{\gamma L_i}{2}(\mathbf{1} - \mathbf{t}_i\mathbf{t}_i)\right)\right\}. \qquad \text{(S9)}$$

It follows from Equation (S9) that, when dynein-motor forces dominate, the centrosome velocity is independent of dynein density.

The time scale for centrosome centering can be estimated by considering a displacement of the centrosome from the cell center by a small distance ε along the *x*-axis. The force balance in the *x* direction is

$$\langle F_x \rangle_\theta = \rho f_0 \left\{\langle L(\theta)\cos\theta\rangle_\theta - \frac{v_{c,x}}{v_0}\langle L(\theta)\cos^2\theta\rangle_\theta\right\} - \frac{\rho\gamma v_{c,x}}{2}\langle L(\theta)\sin^2\theta\rangle_\theta \qquad \text{(S10)}$$

where $\langle \ldots \rangle_\theta$ represents the mean over a uniform angular distribution and $L(\theta)$ is the length of the microtubule spanning the distance between the centrosome and the cell periphery.

For small displacements from the center of a circular cell, $L(\theta) \simeq R - \varepsilon\cos\theta$. Evaluating the moments of L in Equation (S10) to lowest order in ε/R,

$$\langle F_x \rangle_\theta = \rho f_0 \left\{-\frac{1}{2}\varepsilon - \frac{v_{c,x}}{v_0}\left(\frac{R}{2}\right)\right\} - \frac{\rho\gamma v_{c,x}}{2}\left(\frac{R}{2}\right) = 0. \qquad \text{(S11)}$$

Equation (S11) can be solved for $v_{c,x}$ to yield a linear relaxation equation for the displacement ε in terms of its time derivative $d\varepsilon/dt = v_{c,x} = -\varepsilon/\tau_c$, where the relaxation time for centrosome centering is given by

$$\tau_c = R\left(\frac{1}{v_0} + \frac{\gamma}{2f_0}\right). \qquad \text{(S12)}$$

Significantly, τ_c, which is the characteristic time for the centrosome to center, is predicted to depend only on the cell size and molecular parameters, not the number of microtubules. Different cell shapes only affect this result to a numerical pre-factor. For the parameters we have chosen, $\tau_c = 24$ min, assuming a circular cell with the same area as the BCE cells.

REFERENCES

Bicknese, S., Periasamy, N., Shohet, S.B., and Verkman, A.S. (1993). Cytoplasmic viscosity near the cell plasma membrane: measurement by evanescent field frequency-domain microfluorimetry. Biophys J *65*, 1272-1282.

Fushimi, K., and Verkman, A.S. (1991). Low viscosity in the aqueous domain of cell cytoplasm measured by picosecond polarization microfluorimetry. J Cell Biol *112*, 719-725.

Gliksman, N.R., Skibbens, R.V., and Salmon, E.D. (1993). How the transition frequencies of microtubule dynamic instability (nucleation, catastrophe, and rescue) regulate microtubule dynamics in interphase and mitosis: analysis using a Monte Carlo computer simulation. Mol Biol Cell *4*, 1035-1050.
Holy, T.E., Dogterom, M., Yurke, B., and Leibler, S. (1997). Assembly and positioning of microtubule asters in microfabricated chambers. Proc Natl Acad Sci U S A *94*, 6228-6231.
Howard, J. (2001). Mechanics of Motor Proteins and the Cytoskeleton, Sunderland, MA: Sinauer.
Ladd, A.J.C., and Misra, G. (2009). A symplectic integration method for elastic filaments. J Chem Phys *130*, 124909.
Landau, L.D., and Lifshitz, E.M. (1986). Theory of elasticity (Course of Theoretical Phisics): Butterworth–Heinemann.
Love, A.E.H. (1944). A treatise on the mathematical theory of elasticity: Dover.
Shelden, E., and Wadsworth, P. (1993). Observation and quantification of individual microtubule behavior in vivo: microtubule dynamics are cell-type specific. J Cell Biol *120*, 935-945.
Toba, S., Watanabe, T.M., Yamaguchi-Okimoto, L., Toyoshima, Y.Y., and Higuchi, H. (2006). Overlapping hand-over-hand mechanism of single molecular motility of cytoplasmic dynein. Proc Natl Acad Sci U S A *103*, 5741-5745.

FIGURE LEGENDS

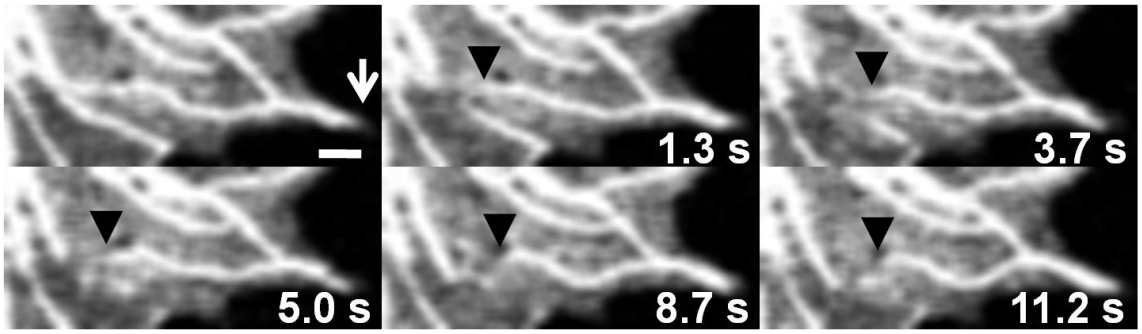

Figure S1. Minus-end microtubules increase in bending after laser severing. A representative example of experiments where a single microtubule, near the cell periphery (white arrow), was severed. Images show increased bending of minus-ended microtubules after severing (cut at black arrow). The plus-end depolymerized at a rate of 0.607 µm/s, while the minus-end depolymerized at a rate of 0.164 µm/s. Note that the plus end depolymerizes but does not show a change in curvature. Scale bar is 1 µm.

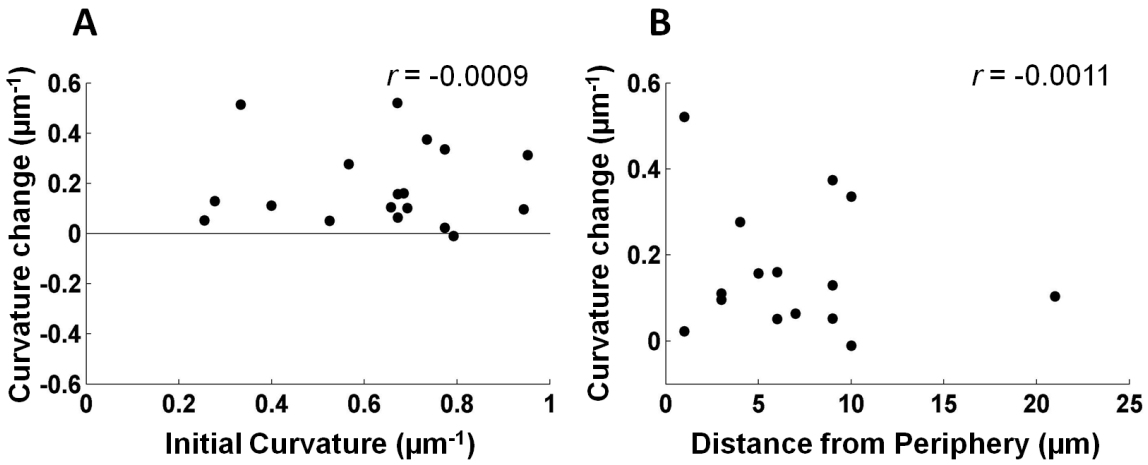

Figure S2. Change in curvature after severing is not correlated with the initial curvature, nor with the spatial location of the cut. (A) The maximum change in RMS curvature for 18 experiments is plotted against the initial curvature. In all experiments that were analyzed, the change in curvature was positive and no correlation with initial curvature was found. (B) The maximum change in RMS curvature is plotted against the shortest distance from the cut to the cell periphery. No significant correlation was observed suggesting that the increase in curvature is not location dependent. In three cells the cuts were positioned under the nucleus and the distance to the periphery could not be determined. *r* is correlation coefficient.

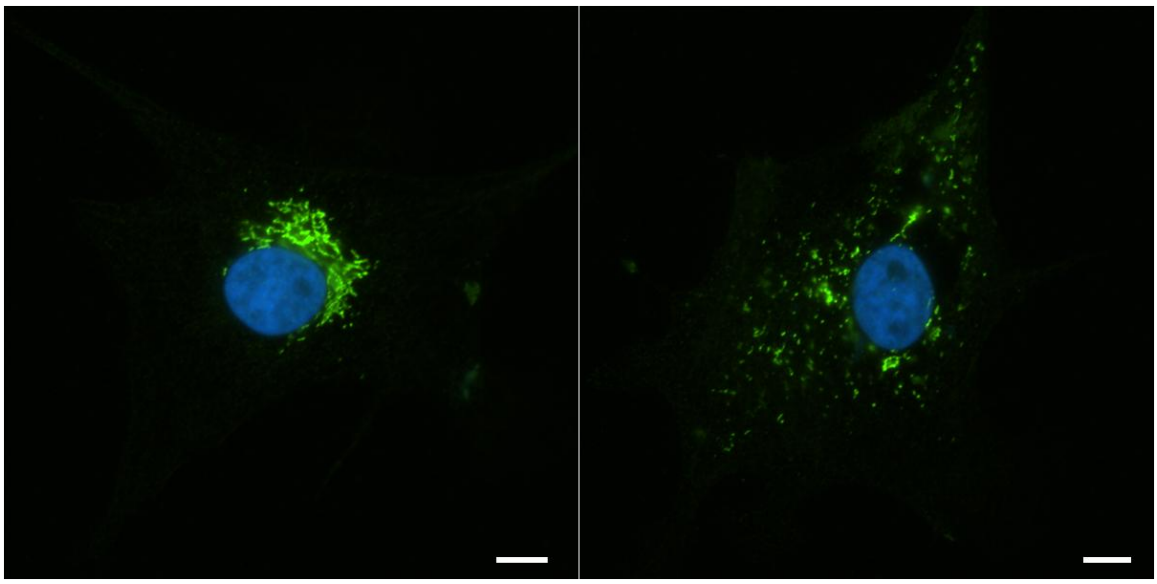

Figure S3. Inhibition of dynein causes dispersion of the Golgi complex. BCE cells were transfected with DsRed-CC1 to inhibit dynein. The cells were then fixed and immunostained with mouse monoclonal Golgi marker (Abcam) and Hoechst 33342. Control cells (left) show a compact Golgi complex (green) near the nucleus (blue), while DsRed-CC1 transfected cells (right) show a dispersed Golgi complex. Scale bars are 10μm.

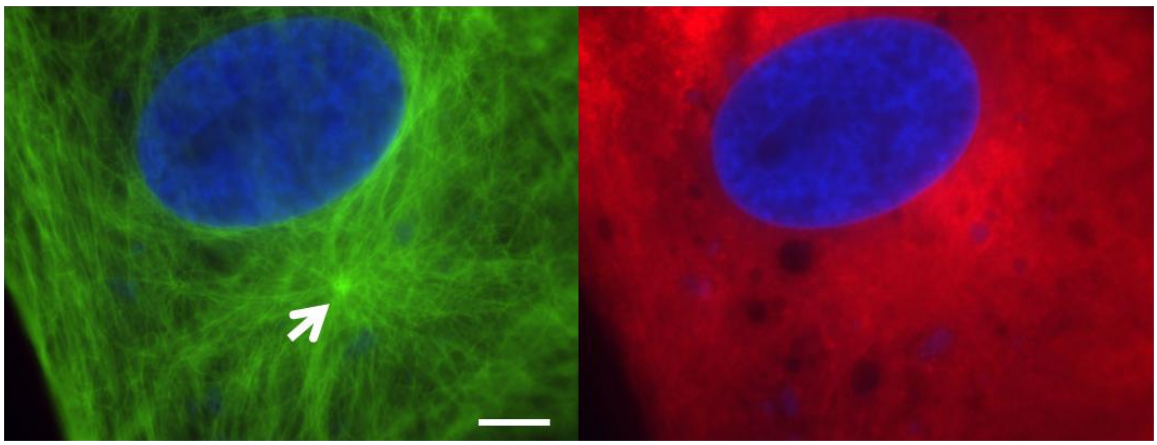

Figure S4. Microtubules radiate from the centrosome in dynein inhibited cells. BCE cells were transfected with DsRed-CC1 and infected with adenoviral GFP-tubulin, and fixed and immunostained with Hoechst 33342 (blue, nucleus). Clear microtubules emanate from the centrosome. Scale bar is 10μm.

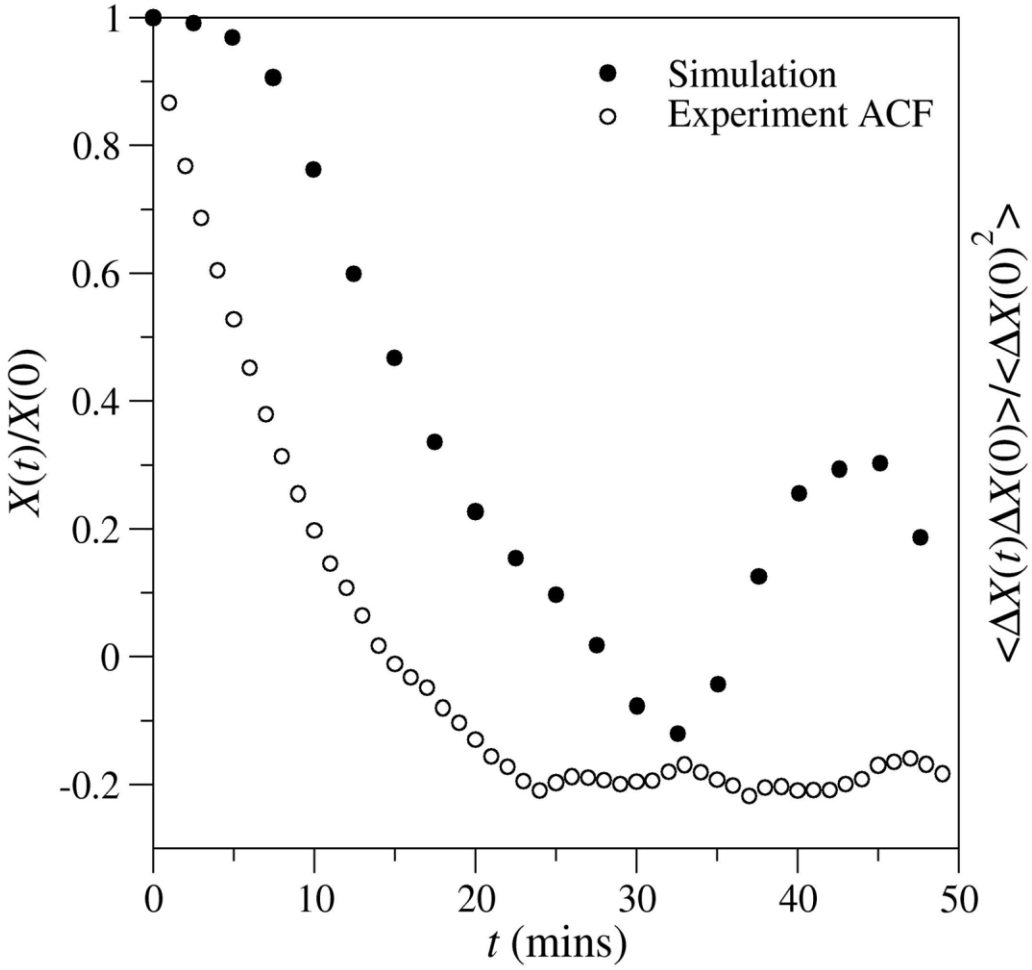

Figure S5. A comparison of centrosome centering (simulation) with the autocorrelation function of fluctuations in centrosome position (experiment). The microtubule network develops during the first 5 min of the simulation; subsequently the centrosome centers with a relaxation time of 12 min. Experimental measurements of the autocorrelation function of the centrosome position decay in about 8 min. The negative region in the autocorrelation function reflects insufficient data to obtain an accurate measurement of the mean position in each cell.

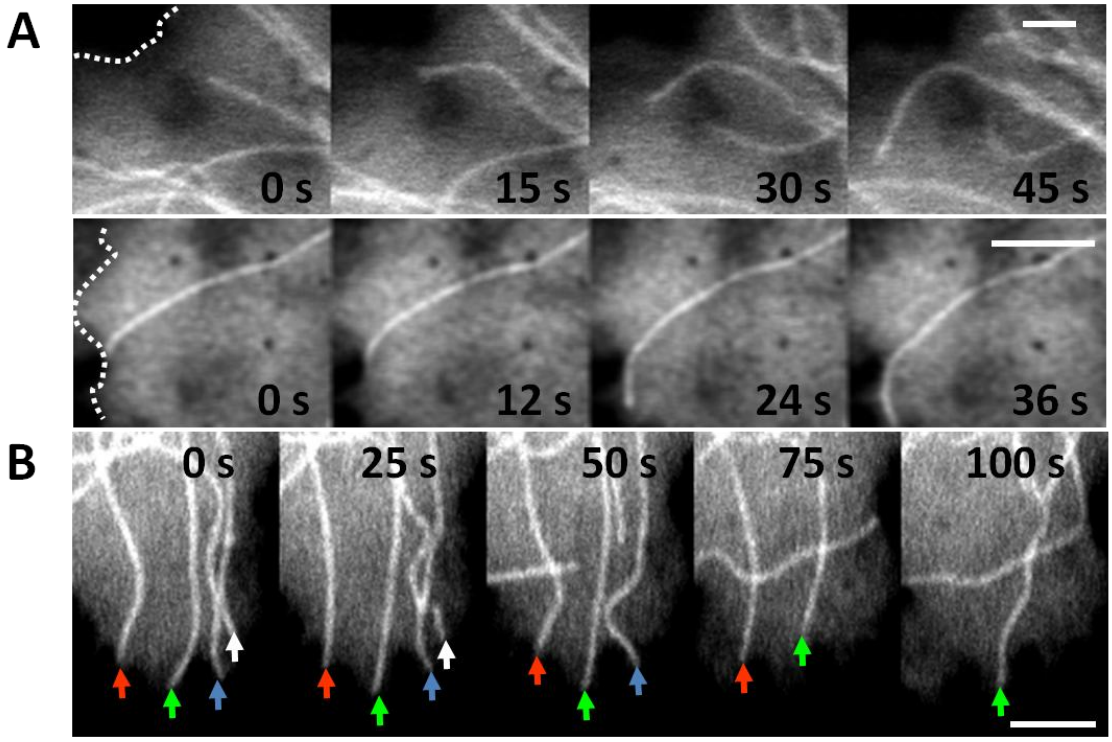

Figure S6. Microtubules undergo three distinct behaviors upon reaching the periphery: (1) buckling with the tip immobilized; (2) sliding along the cell periphery; (3) no growth, eventually depolymerizing. (A) Two examples of microtubules that slide along the cell periphery (dotted white line). (B) Four microtubules (colored arrows) that have reached the cell periphery and remain until they depolymerize. One microtubule (green) does not buckle significantly, suggesting that it has stopped growing. Scale bars are 2.5 µm.

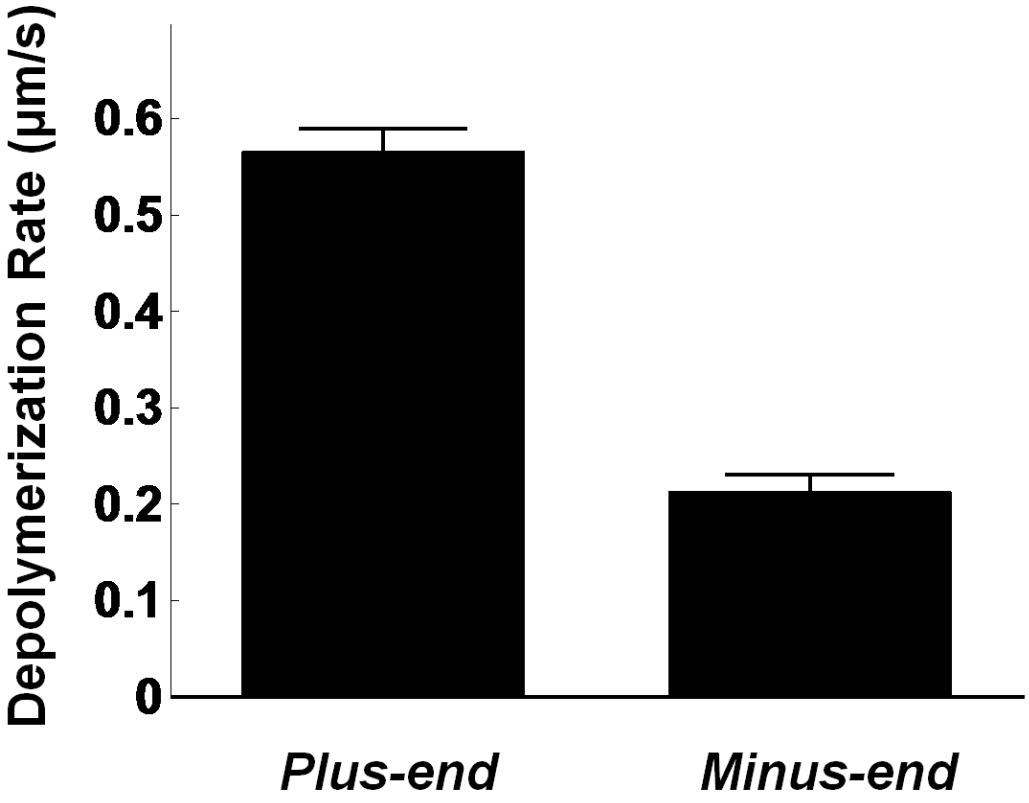

Figure S7. Deploymerization rates of microtubules severed by laser ablation. The bar graphs show that depolymerization rate of the plus-end is consistently larger than that of the minus-end.

MOVIE LENGENDS

Movie S1. Increased bending of minus ended microtubules after severing near the nucleus (Figure 1A). The white arrow indicates the position of the cut.

Movie S2. Straightening of a bent microtubule in a dynein-inhibited cell (Figure 1B).The white arrow indicates the position of the cut.

Movie S3. Simulation of centrosome motion in a normal cell. Dynein motors drive an off-center centrosome towards the center of the cell.

Movie S4. Simulation of centrosome motion in a dynein-inhibited cell. In the absence of motor forces the centrosome remains off center.

Movie S5. Simulation of MTOC motion in a glass cell with short microtubules. The MTOC centers due to pushing forces from short straight microtubules.

Movie S6. Simulation of MTOC motion in a glass cell with long microtubules. The MTOC drifts off center, because the longer microtubules buckle.